THE JOURNAL OF PHYSICAL CHEMISTRY B

ARTICLE

pubs.acs.org/JPCB

Vibrational Softening of a Protein on Ligand Binding

Erika Balog,[†] David Perahia,[‡] Jeremy C. Smith,[§] and Franci Merzel*[,∥]

[†]Department of Biophysics and Radiation Biology, Faculty of Medicine, Semmelweis University, P.O. Box 263. H-1444 Budapest, Hungary

[‡]Bioinformatics, Molecular Dynamics and Modeling, Ecole Normale Superieure de Cachan, 61, av. President Wilson, 94235 Cachan, France

[§]Center for Molecular Biophysics, University of Tennessee/Oak Ridge National Laboratory, P.O. Box 2008, Oak Ridge, Tennessee 37831-6164, United States

[∥]Laboratory for Molecular Modeling, National Institute of Chemistry, Hajdrihova 19, 1000 Ljubljana, Slovenia

ABSTRACT: Neutron scattering experiments have demonstrated that binding of the cancer drug methotrexate softens the low-frequency vibrations of its target protein, dihydrofolate reductase (DHFR). Here, this softening is fully reproduced using atomic detail normal-mode analysis. Decomposition of the vibrational density of states demonstrates that the largest contributions arise from structural elements of DHFR critical to stability and function. Mode-projection analysis reveals an increase of the breathing-like character of the affected vibrational modes consistent with the experimentally observed increased adiabatic compressibility of the protein on complexation.

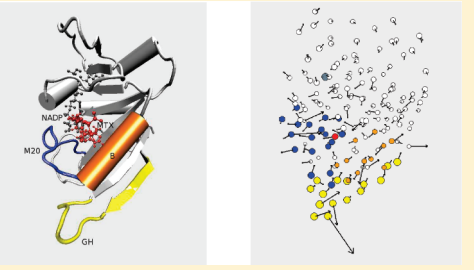

INTRODUCTION

Configurational flexibility is essential for biomolecular activity. In particular, an understanding of the structural and dynamical response of a protein to ligand binding is of fundamental importance. Part of the dynamical response involves changes in the vibrational frequencies of the protein leading to a potentially significant thermodynamic contribution to the binding free energy change.[1,2]

Recent progress on the dynamical effect of ligand binding has been made in studying methotrexate (MTX) binding to dihydrofolate reductase (DHFR).[3] DHFR catalyzes the reduction of dihydrofolate to tetrahydrofolate in the presence of the nicotinamide adenine dinucleotide phosphate (NADPH) cofactor.[3−5] Tetrahydrofolate, in turn, acts as a cofactor in several metabolic processes, for example, in DNA synthesis. Therefore, DHFR has been recognized as a drug target for inhibiting DNA synthesis in rapidly proliferating cells such as cancer cells. MTX is a folate antagonist of DHFR that has been used effectively as a cytotoxic agent in the treatment of cancers.[6] In the dynamical work, neutron scattering experiments showed a shift of the population of the low-frequency region (<20 cm^{-1}) of the vibrational density of states of DHFR on binding MTX, corresponding to dynamical softening.[7] The <20 cm^{-1} region contains modes that tend to be strongly delocalized, collective vibrations. The magnitude of the shift indicated that the vibrational change contributes significantly to the total binding free energy.

In this article, we analyze the vibrational density of states of the holo form of DHFR (DHFR + NADPH) and its complex with MTX (DHFR + NADPH + MTX). Our goal is to reproduce and characterize the experimental vibrational change with an atomic detail model. We reproduce the experimental results and decompose the low-frequency vibrational density of states of complexed DHFR into contributions from selected groups of atoms. Analyzing the polarization of the modes (based on direction and size of atomic displacements) reveals a systematic type of motion characteristic of the modified modes.

METHODS

Molecular Dynamics (MD) Simulation. Crystallographic coordinates were taken from the Protein Data Bank, entry 1RX1 for DHFR + NADPH and 1RX3 for DHFR + NADPH + MTX.[3] Positions for the hydrogen atoms were generated by the HBUILD routine[8] of CHARMM.[9]

MD simulations were carried out with NAMD[10] using the CHARMM all-atom parameter set 22.[11] The simulations were run on eight processors on an SGI Altix 350 machine. NAMD was used due to its efficiency in running in a parallel environment. The preparation of the structures and the analysis of the trajectories were performed with the CHARMM program.[9] The protein, surrounded by the crystallographically identified water molecules, was energy minimized to eliminate unfavorable contacts. Harmonic constraints were applied to heavy atoms to achieve smooth minimization. For the minimization, the steepest descent algorithm was used, with the harmonic force constant decreased every 500 steps and assigned the values 10, 1, and 0.1 kcal/mol/$Å^2$, followed by 200 steps of conjugate gradient minimization with a 0.1 kcal/mol/$Å^2$ force constant. Subsequently, unconstrained minimization was applied for 100 steps with

Received: September 6, 2010
Revised: April 25, 2011
Published: May 10, 2011

steepest descent and for 200 steps with conjugate gradient followed by 1000 steps with the adopted basis Newton−Raphson method (ABNR) as implemented in CHARMM. Both systems were immersed in a rectangular box (68 Å × 58 Å × 55 Å) of explicit water, providing the thickness of at least 10 Å in the x, y, z directions from the protein surface, and were replicated by periodic boundary conditions. The water was modeled by TIP3P.[12] Sodium counterions were added at random positions, and the solvated systems were energy minimized using the same protocol as described above. For the energy calculations, a dielectric constant of 1 was taken. The Particle Mesh Ewald method[13] was used to calculate the electrostatic interactions with a grid spacing of 1 Å or less and order of 6; the real space summation was truncated at 12.0 Å, and the width of the Gaussian distribution was set to 0.34 $Å^{-1}$. van der Waals interactions were reduced to zero by switch truncation operating between 10.0 and 12.0 Å.

The MD simulations were carried out with an integration time step of 1 fs at a temperature of 300 K. The energy-minimized structures were first heated to 300 K with a temperature increment of 10 K after each 1000 steps. At 300 K, a 50 ps constant-temperature equilibration was followed by a 500 ps long constant pressure and temperature (NPT) equilibration using the Nosé-Hoover method.[14,15] After this, a 20 ns NPT production run was carried out.

Twenty snapshots were selected from each trajectory, one per nanosecond. These snapshots compose a representative statistical ensemble of structures and were used together with the CHARMM force field[11] to sample the potential energy surfaces of uncomplexed and complexed DHFR.

The vibrational dynamics was characterized using normal-mode analysis (NMA).[16] The computational complexity of NMA critically depends on the size of the system investigated, i.e., on the total number of atoms in the system including the water. The size of the present systems can most easily be reduced by removing water molecules. However, as the structural and dynamical properties of a protein depend on the hydration water,[17] it is important to keep a sufficient amount of water in the system. To estimate the critical amount of water in the system for the purposes of NMA, we calculated the root-mean-square-distance (rmsd) between the protein atom positions before and after the structural minimization process. It turns out that increasing the thickness of water layer beyond 6 Å does not lead to further relaxation of protein structure on minimization. Hence, the amount of hydration water corresponding to a thickness of 6 Å is sufficient for DHFR to retain the vibrational properties of the fully hydrated protein. The 20 minimized truncated models for the complexed and uncomplexed DHFR were thus constructed, each containing about 1800 water molecules. Minimized structures obtained with the ABNR method were iterated until an energy gradient of 10^{-5} kcal/mol/$Å^2$ was reached and were subjected to NMA as implemented in the program NMscatt[18,19] for the case of the gamma-point (nonperiodic) type of calculation. This procedure led to obtention of all internal vibrational modes of the systems.

Density of States, g(ω). The density of states, $g(\omega)$ is the frequency distribution of the vibrational modes, obtained by solving the eigenvalue problem for the mass-weighted Hessian matrix

$$g(\omega) = \frac{1}{\Delta\omega}\sum_{i=1}^{D}\delta'(\omega-\omega_i) \qquad (1)$$

where $\Delta\omega$ is the width of the sampling interval and

$$\delta'(\omega-\omega_i) = \begin{cases} 1 & \text{if } -\Delta\omega/2 \le \omega-\omega_i < \Delta\omega/2 \\ 0 & \text{otherwise} \end{cases}$$

In 1, D should be in principle the number of vibrational modes, i.e., $3N-6$ (N is the number of atoms in the system), but for the sake of generality, we can set $D = 3N$, assuming 3 translational and 3 rotational modes as vibrational modes with zero frequencies. Distribution $g(\omega)$ corresponds to the density of vibrational states for $\omega > 0$.

To decompose $g(\omega)$ into contributions originating from different parts of the protein, i.e., containing a list of atoms (α_1, α_2), or to determine the contribution from only the protein in the total $g(\omega)$ including also the contribution from the solvent, it is convenient to define the partial atomic vibrational density of states $g_\alpha(\omega)$. For this, we sum all contributions from the selected range of atoms, by weighting by the square of the corresponding mass-weighted atomic displacements

$$g_\alpha(\omega) = \frac{1}{\Delta\omega}\sum_{i=1}^{3N} |\vec{e}_i(\alpha)|^2\delta'(\omega-\omega_i),$$

$$g_{\alpha_1:\alpha_2}(\omega) = \sum_{\alpha_1}^{\alpha_2} g_\alpha(\omega) \qquad (2)$$

where $\vec{e}_i(\alpha)$ is a three-dimensional vector with the x, y, and z components of the mass-weighted displacement of atom α within the normal mode i: $(\vec{e}_i(\alpha) = (e_{ix}(\alpha), e_{iy}(\alpha) e_{iz}(\alpha))$. While the density of states is simply a frequency distribution, and therefore does not contain "contributions" from atoms, it is valid to consider how much, in any given vibration, each individual atom moves. In other words, whereas the density of states is given by the eigenvalues of the normal-mode analysis, to each eigenvalue ω_i is associated an eigenvector $\vec{e}_i$ furnishing the degree of displacement of each atom in the mode. This is what is probed in 2 which is effectively an amplitude-weighted density of states. Formally, 2 is based on the fact that eigenvectors $\vec{e}_i$ form an orthonormal basis in the $3N$-dimensional vector space, so the matrix formed by the eigenvectors $\vec{e}_i$ is unitary. Then, $\sum_{i=1}^{3N}|\vec{e}_i(\alpha)|^2 = \sum_{\alpha=1}^{N}|\vec{e}_i(\alpha)|^2 = 1$. It follows that $g_\alpha(\omega)$ normalizes as: $\int g_\alpha(\omega)d\omega = 3$ and $g(\omega) = \sum_{\alpha=1}^{N} g_\alpha(\omega)$. Our idea of decomposition is that we consider each time the whole system involving the protein, solvent, and ligand if present (the frequencies and eigenvectors are those of the whole system) from which we project-out the corresponding contribution of its constituent part.

The concept of the partial atomic density of states is well-known from solid state physics.[20,21] Moreover, it has been demonstrated recently by Walterfang et al.[22] that the partial vibrational density of states can be measured directly using nuclear resonant inelastic X-ray scattering. Also, the partial vibrational $g(\omega)$ is in fact the quantity determined by inelastic scattering (see ref 23).

Configurational averaging is taken into account by averaging over $g(\omega)$ which are derived for different configurations taken from the MD trajectories.

The present analysis allows information to be derived on participation of selected structural elements in the dynamical relaxation over any given frequency range. To this end we define the average atomic density of states $\bar{g}$, which is a normalized sum of integrated partial atomic densities over the frequency range (ω_1, ω_2)

$$\bar{g} = \frac{1}{\omega_2-\omega_1}\int_{\omega_1}^{\omega_2}\frac{g_{\alpha_1:\alpha_2}(\omega)}{(\alpha_2-\alpha_1)}\,d\omega \qquad (3)$$

Thus, $\bar{g}$ gives information on how much any atom within a selected sequence is on average involved in vibrational dynamics over the given frequency range.

Thermodynamic Properties. NMA does not provide a complete thermodynamic picture of dynamics at physiological temperatures due to the oversimplification of the protein potential energy surface originating from the harmonic approximation. However, the harmonic approximation is reasonable at low temperatures, i.e., well below the glass transition temperature (~200 K), and the experiments with which the present calculations are compared were performed at 120 K.

From the frequency distribution of vibrational modes of the harmonic system it is possible to express vibrational free energy and vibrational entropy following the standard technique of statistical mechanics.[24]

Using the concept of the partial atomic density of states we can write the vibrational entropy of the subsystem, i.e., protein, consisting of N_P atoms as

$$F_P = k_B T \sum_{\alpha=1}^{N_P} \int_0^\infty d\omega g_\alpha(\omega) \left[\frac{\hbar\omega}{2k_B T} + \ln\left(1 - \exp\left(-\frac{\hbar\omega}{k_B T}\right)\right)\right] \quad (4)$$

and analogously the associated vibrational entropy of the subsystem

$$S_P = k_B \sum_{\alpha=1}^{N_P} \int_0^\infty d\omega g_\alpha(\omega) \left[\frac{\hbar\omega}{k_B T}\left(\frac{1}{\exp\left(\frac{\hbar\omega}{k_B T}\right) - 1}\right) - \ln\left(1 - \exp\left(-\frac{\hbar\omega}{k_B T}\right)\right)\right] \quad (5)$$

obtained by integrating over the entire frequency range. When applying the concept of the partial vibrational density of states in the formulas for the entropy and the free energy, it always reproduces the corresponding values of the total system (when $N_P \rightarrow N$). Besides, the definitions 4 and 5 are in agreement with the extensive character of the entropy and free energy: both scale with the size of the system.

Dynamical Properties Projected from the Normal Modes. The softening of the low-frequency modes might be related to a change in the dynamic domain boundaries of the protein on ligand binding. Such an effect, if present, should be manifested in a change of the number of atoms dynamically affected or in a change of the magnitude of atomic displacements in a given mode. To analyze this effect, we define the dynamical activity, $D_{\{L\}}(\omega_i)$ of selected list of atoms L for a given vibrational mode i as the ratio of the average of the squares of atomic displacements of the selected atoms to the average of the squares of all atomic displacements of the protein

$$D_{\{L\}}(\omega_i) = \frac{1/N_{\{L\}} \sum_{\alpha \in \{L\}}^{N_{\{L\}}} |\vec{e}_i(\alpha)|^2}{1/N_P \sum_{\alpha=1}^{N_P} |\vec{e}_i(\alpha)|^2} \quad (6)$$

The larger the deviation of $D_{\{L\}}(\omega_i)$ from 1, the more average atomic displacements of the selected list of atoms differ from the average atomic displacements of the protein within the mode i. N_P is the number of protein atoms.

Further useful information provided by NMA is the directionality and the size of atomic displacements in a given vibrational mode. These can also be analyzed to determine any systematic motion within a molecule associated with the low-frequency modes (<100 cm^{-1}). For some biomolecules, low-frequency modes may be related to biological function such as, for example, the breathing-like motion accompanying bubble formation in DNA[25] or concerted movements of different secondary structures involved in the binding process of the protein PDZ.[26]

Breathing modes can be related to the susceptibility of the system to change its volumetric properties, which implies a connection between their presence and the increased compressibility of the system. Increased adiabatic compressibility of DHFR complexed with MTX relative to the holo form has been reported on the basis of sound velocity and density measurements.[27] Here we examine whether this increase is inherent in the change of the internal dynamics of DHFR upon ligand binding.

The breathing character of mode i with frequency ω_i can be quantified by means of some function distinguishing the radial in-phase displacements of participating atoms. We propose a projection function, R, as the absolute value of the sum of individual atomic displacements $\vec{e}_i(\alpha)$ projected on the radial direction as follows

$$R(\omega_i) = \frac{1}{N_P}\left| \sum_{\alpha=1}^{N_P} \frac{\vec{e}_i(\alpha)}{|\vec{e}_i(\alpha)|} \cdot \frac{\vec{\rho}_\alpha}{|\vec{\rho}_\alpha|} \right| \quad (7)$$

The summation runs over all N_P protein atoms α, and $\vec{\rho}_\alpha/|\vec{\rho}_\alpha|$ is the radial direction, where $\vec{\rho}_\alpha = \vec{r}_\alpha - \vec{R}$. Here, $\vec{R}$ denotes the center of mass of the protein and $\vec{r}_\alpha$ the position of atom α. The ideal breathing mode, possessing only in-phase radial displacements, would be characterized by $R = 1$, while a mode of completely nonbreathing character corresponds to $R = 0$.

RESULTS

We first compare the vibrational density of states, $g(\omega)$, derived from neutron scattering experimental data[7] and from the normal-mode analysis. As the number of atoms in the systems representing the complexed and uncomplexed DHFR differs, due to the presence of the ligand, and because of the variable number of water models in different frames, we can not compare directly $g(\omega)$ of the entire system. Instead, we use 2 to isolate contributions from only the protein atoms in both systems, $g_P(\omega) = \Sigma_{\alpha=1}^{N_P} g_\alpha(\omega)$. Although the vibrational density of states itself is not a sum of contributions from individual atoms, the function that neutrons measure is weighted by the cross-section and eigenvectors as can be inferred from eq 27 of reference 23. Figure 11 of the above reference demonstrates that, for low-frequency modes of a protein, the spherically averaged neutron density of states is similar in form to the unweighted frequency distribution. Hence, the comparison of the density of states corresponding to the protein atoms only with experiment is appropriate. The results obtained from the simulations are shown in Figure 1b and clearly indicate a significant difference in the low-frequency range, below 30 cm^{-1}. The increase of the low-frequency $g_P(\omega)$ of complexed DHFR relative to the uncomplexed DHFR is in excellent agreement with the experimental neutron scattering data in Figure 1a. $g_P(\omega)$ over a broader frequency range is shown in the inset. Again, the experimental and calculated spectra agree very well. Thus, the dynamical

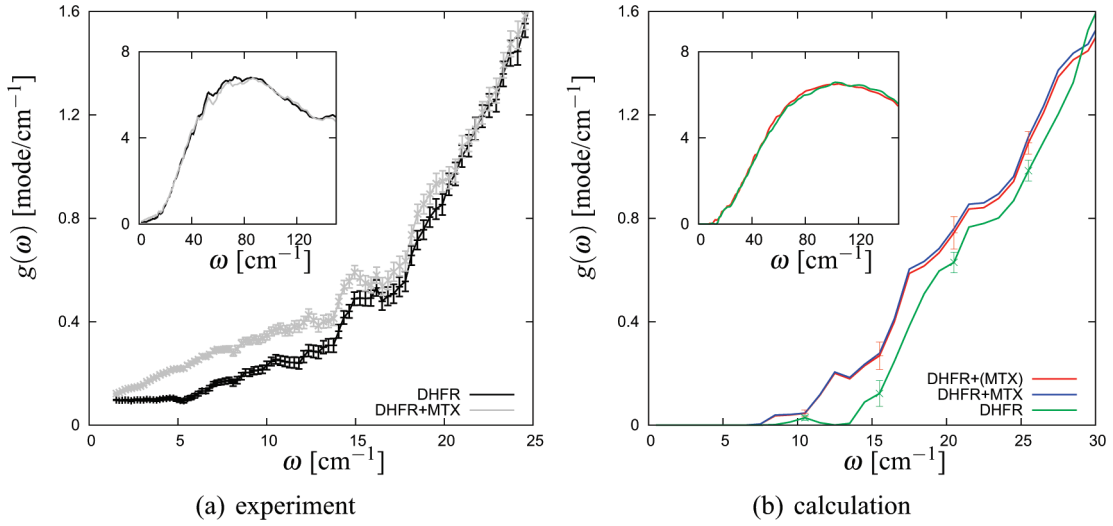

Figure 1. (a) Vibrational density of states $g(\omega)$ for uncomplexed (black) and complexed forms of DHFR (gray) as measured by neutron scattering.[7] (b) Calculated vibrational density of states $g'(\omega) = \sum_{\alpha=1}^{N'} g_\alpha(\omega)$ obtained from NMA showing the contribution from the protein only ($N' = N_P$): uncomplexed DHFR (green), complexed DHFR (red). For comparison, the $g'(\omega)$ is shown, which takes into account contributions of both the protein and the ligand ($N' = N_P + N_L$) (blue line).

Table 1. Average Atomic Density of States $\bar{g}$ for Segments of Uncomplexed (uc) and Complexed (c) DHFR as Defined by 3 and Integrated over the Frequency Range $[0-\omega_{max}]$, Where ω_{max} = 30 cm^{-1} [a]

segment	residue range	$\bar{g}_{uc} \times 10^{-3}$	$\bar{g}_c \times 10^{-3}$	rel. change [%]
helix-B	25−35	0.31	0.32	3.2
helix-C	44−50	0.27	0.31	13.5
loop-M20	13−24	0.46	0.47	2.1
loop-CD	63−72	0.25	0.30	18.2
loop-FG	116−132	0.28	0.35	22.6
loop-GH	136−150	0.34	0.41	18.4
remainder	-	0.35	0.35	0.1
solvent	-	0.32	0.33	3.1

[a] Relative change of $\bar{g}$: $(\bar{g}_c - \bar{g}_{uc})/\bar{g}_{uc}$ is shown in the last column.

softening in the low-frequency range upon ligand binding is fully reproduced by the present simulations. We have also calculated $g_{PL}(\omega)$ from both the protein and the ligand, and this is shown by the blue line in Figure 1b. As expected, the vibrational density of states of the complexed protein does not change significantly upon adding the contribution from the ligand to the vibrational density of states due to the protein only.

The globular structure of DHFR is comprised of a mixed eight-strand β-sheet flanked by four α-helices and several flexible loops.[3] We now decompose the vibrational change by examining structural elements of DHFR which are believed to play a significant role in the stability and function of this protein.[28−30] These elements comprise helices B (residues 25−35) and C (residues 44−50) and loops M20 (residues 14−24), CD (residues 63−72), FG (residues 116−132), and GH (residues 136−150). The results are given in Table 1. The most pronounced relative vibrational changes on complexation are found in the flexible loops CD, FG, and GH, which, remarkably, contain those residues (Gly-67, Gly-121, and Ala-145) having the largest effects found on DHFR stability and function on site-directed mutagenesis.[31−33] A significant contribution to the softening effect is seen also from the helix C, while loop M-20 and helix B participate less. The contribution of the remainder of the protein, comprising roughly 50% of the protein atoms, averages out to zero. For comparison, the relative change in the average atomic vibrational density of states of the water molecules was also calculated giving a ∼3% low-frequency increase on complexation, demonstrating a propagation of the effect into the solvent.

In Figure 2a the secondary structure of DHFR is shown together with the bound methotrexate and nicotinamide adenine dinucleotide phosphate (NADP). To visualize modes of excitations of low-frequency vibrations, the individual atomic displacements were projected onto corresponding centers of mass of each residue. As an example, one of these modes of frequency ω = 13.4 cm^{-1} demonstrates an increased flexibility of loops M20 and GH and is shown in Figure 2b.

The definition of thermodynamic quantities based on the partial atomic density of states, as given by 4 and 5, allows us to calculate the changes of vibrational free energy and entropy associated with the protein. The results are, as expected, in agreement with those calculated from the experimental $g(\omega)$[7] (Table 2). Both experiment and simulation indicate that ligand binding is associated with a large increase of vibrational entropy, making a significant contribution to the free energy change, favoring complexation. The net entropy gain on binding is also in agreement with a recent simple analytical "ball and spring" model of ligand binding.[34]

It is useful to analyze possible changes in the dynamic domain boundaries on ligand binding in terms of the distance from the ligand. We categorize the protein atoms in five groups: (1) atoms up to 5 Å from the closest ligand atom, (2) atoms 5−10 Å from the closest ligand atom, (3) 10−15 Å, (4) 15−20 Å, and (5) atoms that are more than 20 Å from the ligand. These groups form five lists of atoms $\{L\}$, which represent ∼10%, ∼25%, ∼35%, ∼25%, and ∼5% of protein atoms, respectively. As we refer to the modes ω_i < 30 cm^{-1} as low-frequency modes, we calculate dynamic activity defined by 6 as the average overall modes of complexed and uncomplexed DHFR with frequencies below 30 cm^{-1}: $\langle D_{\{L\}}(\omega_i)\rangle_i = 1/N_i \sum_{i=1}^{N_i} D_{\{L\}}(\omega_i)$. Given that the

dx.doi.org/10.1021/jp108493g |J. Phys. Chem. B 2011, 115, 6811–6817

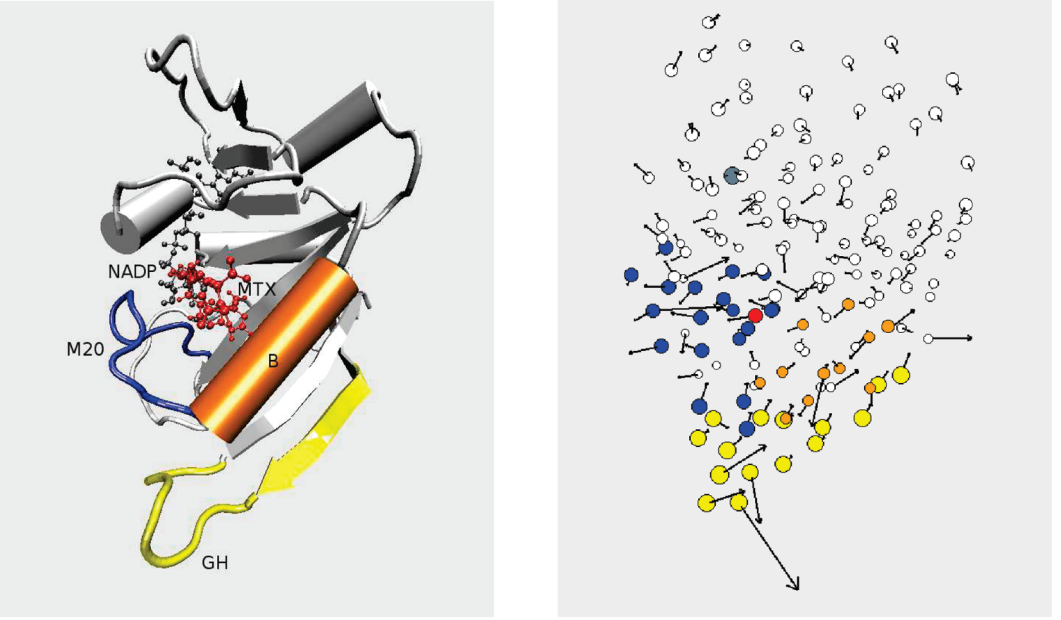

(a) Secondary structure of DHFR (b) bead representation of vibrational mode

Figure 2. (a) Secondary structure of DHFR complexed with MTX (red) and NADP (gray). Orange cylinder and blue and yellow loops correspond to helix-B, loop M20, and loop GH, respectively, as listed in Table 1. (b) Cumulative representation of atomic displacements projected onto the center of mass of the residues for mode no. 9 of frequency ω = 13.4 cm^{-1}. Each bead represents a protein residue or a molecule (NADP/MTX). Colored beads correspond to selected segments in (a).

Table 2. Change of Vibrational Free Energy and Entropy of DHFR on Ligand Binding Calculated at T = 120 K[a]

	simulation	experiment
ΔF [kJ/mol]	-6.2 ± 2.0	-3.5 ± 0.8
$T\Delta S$ [kJ/mol]	8.9 ± 2.2	7.3 ± 1.5

[a] $\Delta F = F_c - F_{uc}$, $\Delta S = S_c - S_{uc}$, where subscript c refers to complexed and uc to uncomplexed DHFR. Experimental values are based on results of ref 7. The experimental $g(\omega)$ was determined at 120 K.

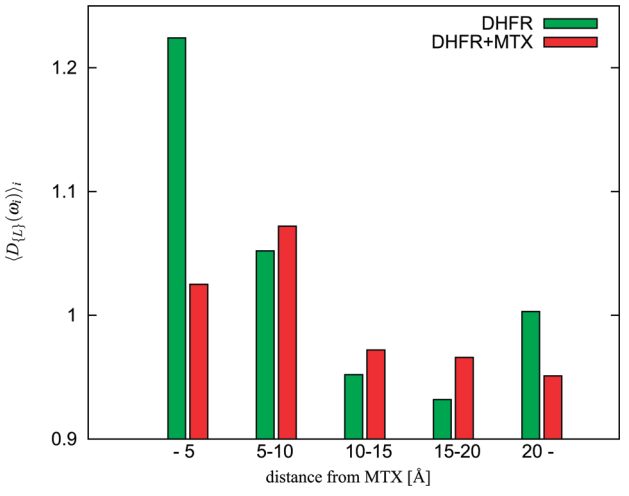

Figure 3. Dynamical activity of protein atoms grouped according to distance from the ligand.

rmsd between complexed and uncomplexed DHFR is small, the lists of atoms {L} are the same for complexed and uncomplexed

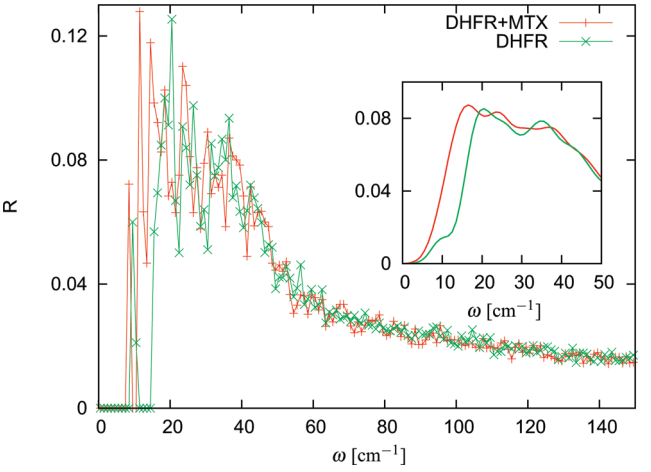

Figure 4. Radial ("breathing") character, R, as a function of mode frequency for complexed (red) and for uncomplexed (green). The inset shows R smoothed by a Gaussian function.

DHFR. The results are shown in Figure 3. Figure 3 shows that the flexibility of the atoms in the binding site of the uncomplexed DHFR is significantly higher than the rest of the protein. On binding MTX the flexibility of these atoms is reduced due to interaction with the ligand and is delocalized away from the binding site as evidenced by the observed increase of the dynamical activity of subsequent layers of atoms in Figure 3. We conclude that the expansion of the domain boundary away from the binding site on ligand binding might be one of the factors causing the softening of the low-frequency modes.

Using the projection operator defined by 7 we now evaluate the breathing-like character of the modes in the system. The

dx.doi.org/10.1021/jp108493g |J. Phys. Chem. B 2011, 115, 6811–6817

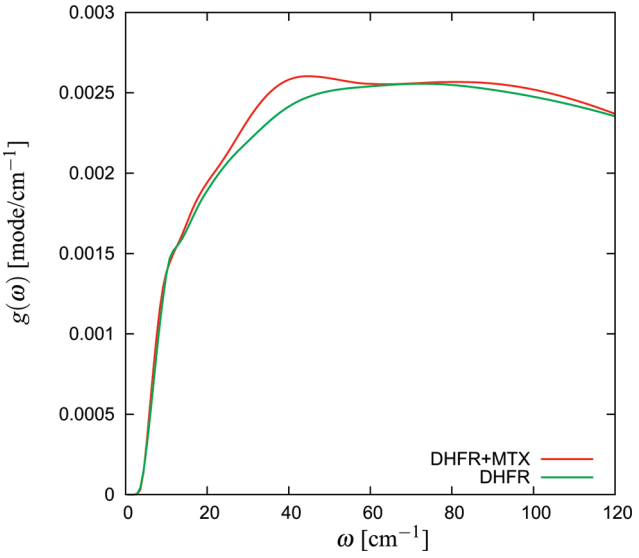

Figure 5. Quasiharmonic analysis of C_α-atoms motion based on 20 ns MD trajectory at 300 K.

distribution function of the radial character is plotted versus frequency in Figure 4. There is a broad maximum at 10−60 cm^{-1} in both systems. Furthermore, for complexed DHFR at frequencies <20 cm^{-1}, there is a significant shift of the profile toward larger R values (see Figure 4, inset). This means that on ligand binding the dynamical character of the low-frequency modes becomes more breathing-like. The increase of the breathing-like character can be interpreted as an enhancement of the degrees of freedom responsible for volumetric changes of the protein, consistent with increased compressibility of the system. Indeed, the adiabatic compressibility of complexed DHFR has been found experimentally to be significantly higher than for the uncomplexed protein.[27]

The present calculations concern a comparison between experiment and calculation at 120 K. For hydrated proteins at physiological temperatures, a significant contribution to the atomic mean-square displacements arises from anharmonic dynamics. These anharmonic motions, together with overdamping of the low-frequency modes, result in quasielastic neutron scattering that renders difficult the derivation of model-independent thermodynamic quantities from experimental data. It is conceivable that anharmonic degrees of freedom might also be modified on ligand binding. A "quasiharmonic" analysis (QHA)[16] includes anharmonic effects present only at higher temperatures. The QHA results of the C_α motion for complexed and uncomplexed DHFR derived from 20 ns MD trajectory at 300 K are given in Figure 5. We observe that the softening is still present, but at higher frequencies. However, we shall note that the length of the MD trajectory of 20 ns used in the QHA might not be sufficient to describe $g(\omega)$ accurately at low frequencies.

CONCLUSIONS

The experimentally observed increase of the vibrational flexibility of DHFR on binding of the ligand methotrexate is quantitatively reproduced here using normal-mode analysis. In comparison, previous calculations were in only qualitative agreement.[34,35] The success of the present calculations is most likely due to the explicit hydration water taken into account in the NMA. However, the present results cannot be generalized to other proteins and ligands since the effect depends on the strength of the interactions involved. Furthermore, the present analysis concentrates on the harmonic component of the dynamics. Anharmonic motions, which become significant for T > ∼200 K, can be restricted by ligand binding, and this is likely to be at the origin of the flexibility decrease observed by NMR and crystallography on binding small organic ligands to some proteins.[36,37]

The most significant softening of vibrational dynamics on complexation of DHFR with MTX is found in the loops of the protein containing the residues Gly-67, Gly-121, and Ala-145, which have been shown by mutagenesis to be crucial for the enzyme function.[31−33]

We observe the expansion of the dynamic domain boundary away from the binding site on ligand binding which might be one of the factors causing the softening of the low-frequency modes.

The low-frequency modes of the protein contain considerable radial (breathing) character, and these modes are affected by ligand binding. This demonstrates that the system becomes prone to deformation of the structure enabling change of the volume of the molecule, consistent with the adiabatic compressibility of complexed DHFR being higher than that of the holo form. Hence, the presence of breathing modes in globular proteins may make an important intrinsic contribution to protein compressibility.[38]

AUTHOR INFORMATION

Corresponding Author
*E-mail: franc@cmm.ki.si.

ACKNOWLEDGMENT

The authors acknowledge the following support: E.B. and F.M. from the Slovenian-Hungarian scientific and technological intergovernmental grant (SI-8/2008), F.M. from grant P1-0002 of the Slovenian Research Agency, D.P. from the Centre National de la Recherche Scientifique (CNRS), and J.C. from the National Science Foundation grant number MCB-0842871.

REFERENCES

(1) Tidor, B.; Karplus, M. *J. Mol. Biol.* **1994**, *238*, 405–414.
(2) Fischer, S.; Smith, J. C.; Verma, C. S. *J. Phys. Chem. B* **2001**, *105*, 8050–8055.
(3) Sawaya, M. R.; Kraut, J. *Biochemistry* **1997**, *36*, 586–603.
(4) Epstein, D. M.; Benkovic, S. J.; Wright, P. E. *Biochemistry* **1995**, *34*, 11037–11048.
(5) Howell, E. E.; Villafranca, J. E.; Warren, M. S.; Oatley, S. J.; Kraut, J. *Science* **1986**, *231*, 1123–1128.
(6) Huennekens, F. M. *Adv. Enzyme Regul.* **1994**, *34*, 397–419.
(7) Balog, E.; Becker, T.; Oettl, M.; Lechner, R.; Daniel, R.; Finney, J.; Smith, J. C. *Phys. Rev. Lett.* **2004**, *93*, 028103.
(8) Brunger, A. T.; Karplus, M. *Proteins: Struct, Funct, Bioinf.* **1988**, *4*, 148–156.
(9) Brooks, B. R.; Bruccoleri, R. E.; Olafson, B. D.; States, D. J.; Swaminathan, S.; Karplus, M. *J. Comput. Chem.* **1983**, *4*, 187–217.
(10) Phillips, J. C.; Braun, R.; Wang, W.; Gumbart, J.; Tajkhorshid, E.; Villa, E.; Chipot, C.; Skeel, R. D.; Kale, L.; Schulten, K. *J. Comput. Chem.* **2005**, *26*, 1781–1802.
(11) MacKerell, A. D.; Bashford, D.; Bellott, M.; Dunbrack, R. L. J.; Evanseck, J. D.; Field, M. J.; Fischer, S.; Gao, J.; Ha, S.; Joseph-McCarthy, D.; Kuchnir, L.; Kuczera, K.; Lau, F. T. K.; Mattos, C.; Michnick, S.; Ngo, T.; Nguyen, D. T.; Prodhom, B.; Reiher, W. E. I.; Roux, B.; Schlenkrich, M.; Smith, J. C.; Stote, R.; Straub, J.; Watanabe,

M.; Wiorkiewicz-Kuczera, J.; Yin, D.; Karplus, M. *J. Phys. Chem. B* **1998**, *102*, 3586–3616.
(12) Jorgensen, W. L.; Chandrasekhar, J.; Madura, J. D.; Impey, R. W.; Klein, M. L. *J. Chem. Phys.* **1983**, *79*, 926–935.
(13) Feller, S. E.; Pastor, R. W.; Rojnuckarin, A.; Bogusz, S.; Brooks, B. R. *J. Phys. Chem.* **1996**, *100*, 17011–17020.
(14) Nose, S. *Mol. Phys.* **1984**, *52*, 255–268.
(15) Hoover, W. G. *Phys. Rev. A* **1985**, *31*, 1695–1697.
(16) Brooks, B. R.; Janežič, D.; Karplus, M. *J. Comput. Chem.* **1995**, *16*, 1522–1542.
(17) Smith, J. C.; Merzel, F.; Bondar, A. N.; Tournier, A.; Fischer, S. *Phil. Trans. R. Soc. London B* **2004**, *359*, 1181–1190.
(18) Merzel, F.; Fontaine-Vive, F.; Johnson, M. R. *Comput. Phys. Commun.* **2007**, *177*, 530–538.
(19) Meinhold, L.; Merzel, F.; Smith, J. C. *Phys. Rev. Lett.* **2007**, *99*, 138101.
(20) Jin, W.; Vashishta, P.; Kalia, K. *Phys. Rev. B* **1993**, *48*, 9359–9368.
(21) Thorpe, M. F.; de Leeuv, S. W. *Phys. Rev. B* **1986**, *33*, 8490–8505.
(22) Walterfang, M.; Keune, W.; *Phys. Rev. B* **2005**, *71*, 035309–1−9.
(23) Smith, J. C.; Cusack, S.; Pezzeca, U.; Brooks, B.; Karplus, M. *J. Chem. Phys.* **1986**, *85*, 3636–3654.
(24) McQuarrie, D. A. *Statistical Mechanics*; University Science Books: Sausalito, CA, 2000.
(25) Merzel, F.; Fontaine-Vive, F.; Johnson, M. R.; Kearley, G. J. *Phys. Rev. E* **2007**, *76*, 031917.
(26) De Los Rios, P.; Cecconi, F.; Pretre, A.; Dietler, G.; Michielin, O.; Piazza, F.; Juanico, B. *Biophys. J.* **2005**, *89*, 14–21.
(27) Kamiyama, T.; Gekko, K. *Biochim. Biophys. Acta* **2000**, *1478*, 257–266.
(28) Radkiewicz, J. L.; Brooks, C. L., III *J. Am. Chem. Soc.* **2000**, *122*, 225–231.
(29) Agarwal, P. K.; Billeter, S. R.; Rajagopalan, P. T. R.; Benkovic, S. J.; Hammes-Schiffer, S. *Proc. Natl. Acad. Sci. U.S.A.* **2002**, *99*, 2794–2799.
(30) Loveridge, E. J.; Tey, L. H.; Allemann, R. K. *J. Am. Chem. Soc.* **2010**, *132*, 1137–1143.
(31) Gekko, K.; Kunori, Y.; Takeuchi, H.; Ichihara, S.; Kodama, M. *J. Biochem.* **1994**, *116*, 34–41.
(32) Ohmae, E.; Iriyama, K.; Ichihara, S.; Gekko, K. *J. Biochem.* **1996**, *119*, 703–710.
(33) Ohmae, E.; Ishimura, K.; Iwakura, M.; Gekko, K. *J. Biochem.* **1998**, *123*, 839–846.
(34) Moritsugu, K.; Njunda, B. M.; Smith, J. C. *J. Phys. Chem. B* **2010**, *114*, 1479–1485.
(35) Balog, E.; Smith, J. C.; Perahia, D. *Phys. Chem. Chem. Phys.* **2006**, *8*, 5543–5548.
(36) Cheng, J. W.; Lepre, C. A.; Moore, J. M. *Biochemistry* **1994**, *33*, 4093–4100.
(37) Fushman, D.; Ohlenschlager, O.; Ruterjans, H. *J. Biomol. Struct. Dyn.* **1994**, *11*, 1377–1402.
(38) Dadarlat, V. M.; Post, C. B. *Biophys. J.* **2006**, *91*, 4544–4554.